

PUTTING IMAGES ON A MANIFOLD FOR ATLAS-BASED IMAGE SEGMENTATION

Yihui Cao, Yuan Yuan, Xuelong Li, Pingkun Yan

Center for OPTical IMagery Analysis and Learning (OPTIMAL), State Key Laboratory of Transient Optics and Photonics, Xi'an Institute of Optics and Precision Mechanics, Chinese Academy of Sciences, Xi'an 710119, Shaanxi, P. R. China

ABSTRACT

In medical image analysis, atlas-based segmentation has become a popular approach. Given a target image, how to select the atlases with the similar shape of anatomical structure to the input image is one of the most critical factors affecting the segmentation accuracy. In this paper, we propose a novel strategy by putting the images on a manifold to analyze the intrinsic similarity between the images. A subset of atlases can be selected and the optimal fusion weights are computed in a low-dimensional manifold space. Finally, it combines the selected atlases by using the corresponding weights for image segmentation. The experimental results demonstrated that our proposed method is robust and accurate especially when a large number of training samples are available.

Index Terms— image segmentation, atlas-based, manifold learning, fusion.

1. INTRODUCTION

In medical image analysis, automatic or semi-automatic segmentation of anatomical structures is a fundamental task. Pham *et al.* [1] classified the common approaches into eight categories. Among the reported methods, both deformable models [2] and atlas-based approaches use the information of the boundary of anatomical structures. Atlas-based segmentation methods, for its high accuracy, have been extensively applied for segmenting MR brain images [3] and prostate images [4].

In the classical methods of atlas-based segmentation, the first step is registration that each atlas image is aligned with the query image. The closest atlas is then selected for the segmentation of a particular image. It was shown that atlas selection strategies were the key factors directly affecting the final segmentation accuracy [5]. In the previous reports, there were different atlas selection strategies. For example, Wu *et al.* [6] selected a ‘best’ similar atlas by measuring the Normalized Mutual Information (NMI) of images. In a similar work [4], it was based on a multi-atlas selection method and fused the selected atlases for segmentation. These methods were seen as directly using Euclidean distance to analyze the

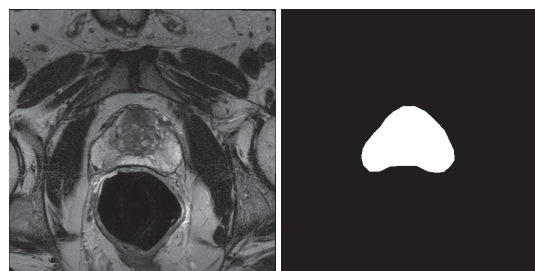


Fig. 1. The left is a MR image of prostate. The right is a binary labeled image segmented by the expert. An atlas is defined as a pair of these two images.

similarity in global image space. However, in the global image space, the measure by geodesic distance can better reflect the intrinsic similarity than direct Euclidean distance.

Fig. 1 shows an atlas with corresponding segmentation. It can be imagined that if the shape of anatomical structure of query image is highly similar to the image on the left, the query image can be segmented by the binary labeled image on the right. So selecting the similar images is very important for the work of atlas-based image segmentation. Directly analyzing the similarity of images in image space is difficult and inaccurate because of the interference of redundant information. In this paper, we propose a novel atlas selection strategy based on manifold learning, which projects the image space into a low-dimensional space. The similarity of images reflected by geodesic distance in image space can be approximately estimated by the simple Euclidean distance in the low-dimensional space, for that the projection preserves the local neighborhood of images. Our main contributions in this paper are included as follows: 1) By putting the images on a manifold, the intrinsic similarity of images can be reflected in a low-dimensional space; 2) We propose a novel algorithm for computing the optimal fusion weights of the selected atlases by solving a cost function of minimal reconstruction error. We compare our method with the state-of-the-art methods [4, 6] based on the performance. The results show that our method is robust and promising.

The rest of this paper is organized as follows: In section 2, we give a detailed description of our method. Our data sets

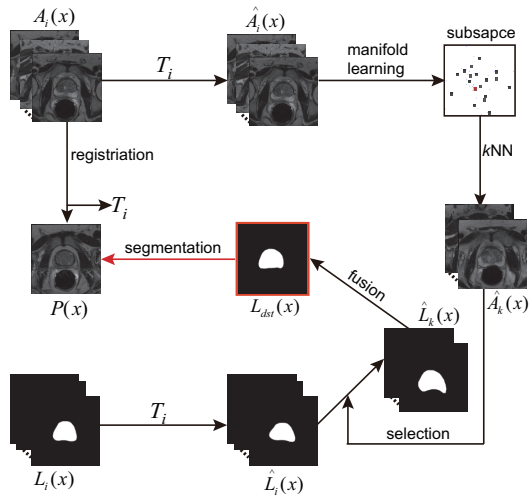


Fig. 2. An overview of our proposed method. Note that the destination image for segmentation is marked by the red box.

and some experimental results are discussed in section 3. And some conclusions about this paper are provided in section 4.

2. METHOD

In this section, we give a briefly overview of our proposed method. The workflow is shown in Fig. 2. We define an atlas to be an original MR image $A(x)$ and its corresponding binary labeled image $L(x)$, which is segmented by an expert (where x represents a pixel location in an image).

Given a query image $P(x)$, the problem is how to select atlases with the similar shape of anatomical structure to the query image. In practice, the atlas can not be directly used to segmentation for the large variations of shapes. Generally, each atlas image is firstly aligned to the query image, which makes the shape of atlas closing to the query image. Then a critical step is the similar images selection. In our method we apply manifold learning to address this problem, because of the projection preserving local neighborhood of images in manifold learning. Finally, the selected atlases are fused to a single image for segmentation. The detailed our method is described in following sections.

2.1. Registration

The registration stage includes a rigid registration step and a non-rigid registration step. Firstly, each atlas image $A_i(x)$ ($i = 1, 2, \dots, N$) is matched to the query image $P(x)$ by a translation and rotation transform. After that a B-Spline deformable registration is performed. By the registration, each atlas image corresponds to a parameter of transformation T_i . Applying T_i to $A_i(x)$ and $L_i(x)$ yields the new sets of deformed atlas $\hat{A}_i(x)$ and $\hat{L}_i(x)$. The transformation is de-

scribed as follows:

$$\hat{A}_i(x) = A_i(x) \circ T_i, \quad (1)$$

$$\hat{L}_i(x) = L_i(x) \circ T_i, \quad (2)$$

where the notation “ \circ ” represents a remapping process.

2.2. Atlas selection on manifold

For the interference of redundant information, directly analyzing the similarity of images in image space is difficult and unreliable. We address the problem of atlas selection in a low-dimensional space by the manifold learning. The adjacency graph of atlases in image space can project into a low-dimensional space by preserving the local neighborhood. In this work, all atlases have the same size of m pixels. Each atlas $\hat{A}_i(x)$ is represented by a vector h_i in the m -dimensional space R^m . And the atlas can be considered as a point distributing in the m -dimensional manifold space. Then each vector h_i is linearly mapped to a vector l_i in the n -dimensional space R^n ($n \ll m$). It yields a transformation matrix W in the procession of projection. The query image $P(x)$ is represented by a vector h_0 mapping into the same low-dimensional space as follows:

$$l_0 = W^T \times h_0, \quad (3)$$

where l_0 is a low-dimensional vector that represents the query image.

In light of the projection preserving the local neighborhood, the similarity of images in the low-dimensional space can be estimated by the simple Euclidean distance instead of geodesic distance. The distance of each atlas to the query image is computed as follows:

$$D_i = \|l_0 - l_i\|_2. \quad (4)$$

According to the Euclidean distance D_i , k -Nearest Neighbor (k NN) $\hat{A}_k(x)$ are selected.

2.3. The weights of fusion

With the subset $\hat{A}_k(x)$ selected from the set $\hat{A}_i(x)$, a corresponding subset of labeled images $\hat{L}_k(x)$ can be selected. The destination image $L_{dst}(x)$ for segmentation can be considered as a linear combination of the images $\hat{L}_k(x)$. In the low-dimensional space R^n , labeled images are represented by the vectors l_k and the destination image $L_{dst}(x)$ is l_0 . The optimal linear combination can be solved by a cost function of minimal reconstruction error ε [7]:

$$\arg \min_{\omega_1, \dots, \omega_K} \varepsilon = \|l_0 - \sum_{k=1}^K \omega_k l_k\|_2^2, \quad (5)$$

with a constraints $\sum \omega_k = 1$. Where $\omega = (\omega_1, \dots, \omega_K)$ is the vector of reconstruction weights that the value reflects the

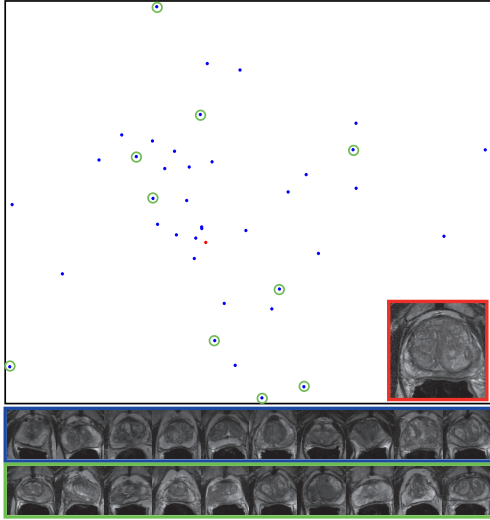


Fig. 3. The upper part of the graph shows the distribution of the atlases (blue points) and the query image (red point) in 2-dimensional space, and the query image is shown in the red box. The lower part of the figure visualizes ten of nearest atlases selected based our method in the blue box. Ten atlases in the green box are selected based on maximum NMI, and their positions in our 2D manifold are described by green circles in the upper part.

contribution of each image $\hat{L}_k(x)$ to the destination image $L_{dst}(x)$. Apparently, to minimize the reconstruction error is equal to address a constrained least squares problem. So we introduce a Gram matrix G :

$$G = (l_0 \mathbf{1}^T - L)^T (l_0 \mathbf{1}^T - L), \quad (6)$$

where $\mathbf{1}$ is a vector of ones with the same size of l_0 , L consists of the K vectors of the labeled images. Then the problem can be solved by the following solution:

$$\omega = \frac{G^{-1} \mathbf{1}}{\mathbf{1}^T G^{-1} \mathbf{1}}. \quad (7)$$

Finally, we use the simple robust Majority Voting fusion method [5] to fuse the labeled images $\hat{L}_k(x)$ into a single destination image $L_{dst}(x)$ for segmentation. The Majority Voting method is defined as follows:

$$L_{dst}(x) = \sum_{k=1}^K \omega_k \hat{L}_k(x), \quad (8)$$

where $\omega = (\omega_1, \dots, \omega_K)$ is the vector of fusion weights, it is defined in equation (5).

3. EXPERIMENTS

3.1. Data and evaluation criterion

The performance of our method is evaluated on 40 MR images of the prostate, which were taken from 40 different pa-

tients. The size of each image is 512×512 pixels and with a binary image for the ground truth segmented by the expert. For the relatively limited data, a leave-one-out cross-validation approach is applied. The final segmentation overlap is measured by the Dice Similarity Coefficient (DSC), as given below:

$$DSC(A, B) = \frac{2|A \cap B|}{|A| + |B|}, \quad (9)$$

where A is a binary label image as the ground truth, B is the automatically segmented binary image. $|\cdot|$ denotes the number of pixels in a object region. The value varies between 0 and 1, and the higher value indicates the better segmentation.

3.2. Manifold learning by LPP

There were many classical algorithms of manifold learning, such as the linear projection of Principal Component Analysis (PCA) and the nonlinear ISOMAP [8] and LLE [9] algorithms. In our experiment, we apply the Locality Preserving Projections (LPP) [10] algorithm. LPP has both the advantage of linear and nonlinear techniques. It can linearly project high-dimensional data into a low-dimensional space and preserve local neighborhood information.

In this work, we extracted the region of interest in the atlas with the size of 256×256 pixels around the image center. That is to say, h_i represents a point in the 65536-dimensional space. Before the projection, all images are preprocessed by histogram equalization to reduce the impact of light. In Fig. 3, the upper part of figure shows the distribution of atlases in the 2D manifold space. The red point represents the query image, and the blue points represent the atlases image. And the region of interest of the query image is showed in the red box. The lower part of the figure respectively visualizes ten nearest atlases selected based on our method, and shown in the blue box. In the green box, it shows ten images selected based on the method [5]. And the position of these images is described by green circles in the upper part. It can be seen, the shape of images in blue box is more similar to in red box than in green box. And in the 2D manifold space, the positions of these images in blue box are nearer to in red box than in green box. That is to say, putting the images on the low-dimensional manifold is helpful for find the similar images. Considering affection of the dimension number about the low-dimensional manifold to the accuracy of segmentation, we test the dimensions from 1 to 39 and find that 38 is the most proper in our experiments.

3.3. Results

We compared our method with two other state-of-the-art methods proposed by Wu *et al.* [6] and Klein *et al.* [4], respectively. The methods were carried out using the same registration. For Wu's method, a 'best' single atlas was selected based on the maximum NMI. In the work of Klein *et*

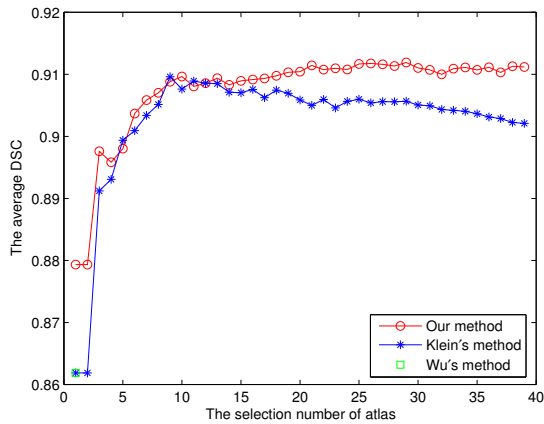


Fig. 4. The average of DSC of three methods.

al. [4], k atlases were selected to fuse for segmentation. In our work, the cross validation leave-one-out approach was employed. One of the 40 images was used as the query image and the rest are used as atlases at each time. The average DSC of 40 experiments is shown in Fig. 4. We selected the nearest single neighbor comparing with Wu's method [6]. The average of DSC based on our method is about 0.88, while it's about 0.86 in Wu's method. When the selection number of atlas is more than one, we compare our method with Klein's. When the selection number ranges from 1 to 39, the DSC values of our method are higher than the Klein's in most cases as shown in Fig. 4. Especially, the problem of over-fitting apparently occurs in Klein's method when the samples exceed a limitation. It can be concluded that our method is superior to Klein's method in the case of relative large sample and is not inferior in the case of small sample.

In Fig. 5, it shows several segmentation results. The qualitative results of Klein's are in top row and our method's are in bottom row. The red contours represent the ground truth. And the yellow contours are automatically delineated by the two methods.

4. CONCLUSION

In this paper, we proposed a novel strategy of atlas selection by putting images on a manifold for analyzing, which reveals the similarity of shape features of atlases in a low-dimensional manifold space. By comparing with two other state-of-the-art methods [4, 6], the experimental results indicate our algorithm is robust and promising. In the future work, we will test our algorithm on other datasets and further extend our work to 3D atlas-based segmentation.

5. ACKNOWLEDGMENTS

The presented research work is supported by the National Basic Research Program of China (973 Program) (Grant No.

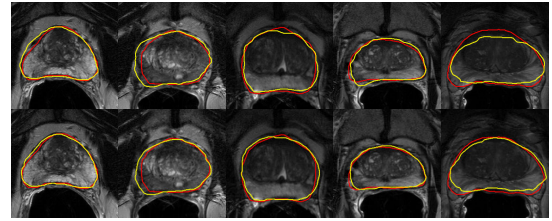


Fig. 5. Segmentation results of Klein's (in top row) and our method (in bottom row). The red contours represent the ground truth. And the yellow contours are automatically delineated by the two methods.

2011CB707000), the National Natural Science Foundation of China (Grant No. 61072093) and the Open Project Program of the State Key Lab of CAD & CG (Grant No. A1116), Zhejiang University.

6. REFERENCES

- [1] D. L. Pham, C. Xu, and J. L. Prince, "Current methods in medical image segmentation," *Annual Review of Biomedical Engineering*, vol. 2, pp. 315-338, 2000.
- [2] P. Yan, S. Xu, B. Turkbey, and J. Kruecker, "Discrete deformable model guided by partial active shape model for TRUS image segmentation," *IEEE Transactions on Biomedical Engineering*, vol. 57, no. 5, MAY 2010.
- [3] M. B. Cuadra, C. Pollo, A. Bardera, O. Cuisenaire, and J. P. Thiran, "Atlas-based segmentation of pathological brain MR images," *ICIP*, pp. 573-576, 2003.
- [4] S. Klein, U. A. van der Heide, I. M. Lips, M. van Vulpen, M. Staring, and J. P. W. Pluim, "Automatic segmentation of the prostate in 3D MR images by atlas matching using localized mutual information," *Medical Physics*, vol. 35, no. 4, pp. 1407-1417, 2008.
- [5] P. Aljabar, R. A. Heckemann, A. Hammers, J. V. Hajnal, D. Rueckert, "Multi-atlas based segmentation of brain images: Atlas selection and its effect on accuracy," *NeuroImage*, vol. 46, pp. 726-738, 2009.
- [6] M. Wu, C. Rosano, P. Lopez-Garcia, C. S. Carter, and H. J. Aizenstein, "Optimum template selection for atlas-based segmentation," *NeuroImage*, vol. 34, no. 4, pp. 1612-1618, 2007.
- [7] H. Chang, D. Y. Yeung, and Y. Xiong, "Super-resolution Through Neighbor Embedding," *CVPR*, vol. 1, pp. 275-282, 2004.
- [8] J. B. Tenenbaum, V. de Silva, and J. C. Langford, "A Global Geometric Framework for Nonlinear Dimensionality Reduction," *Science*, vol. 290, 22 December 2000.
- [9] S. Roweis, and L. K. Saul, "Nonlinear dimensionality reduction by locally linear embedding," *Science*, vol. 290, 22 December 2000.
- [10] X. He and P. Niyogi, "Locality preserving projections," *Neural Information Processing Systems*, 2003.